



Validation of ETWatch using field measurements at diverse landscapes: A case study in Hai Basin of China

Bingfang Wu^{a,*}, Nana Yan^a, Jun Xiong^a, W.G.M. Bastiaanssen^{b,c}, Weiwei Zhu^a, Alfred Stein^d

^a Institute of Remote Sensing Applications (IRSA), Datun Road, Beijing 100101, PR China

^b WaterWatch, Generaal Foulkesweg 28, 6703 BS Wageningen, The Netherlands

^c Delft University of Technology, Stevinweg 1, 2600 GA Delft, The Netherlands

^d Twente University, Hengelosestraat 99, 7514 AE Enschede, The Netherlands

ARTICLE INFO

Article history:

Received 15 September 2011

Received in revised form 11 February 2012

Accepted 21 February 2012

Available online 1 March 2012

This manuscript was handled by Philippe Baveye, Editor-in-Chief, with the assistance of Magdelaine Laba, Associate Editor

Keywords:

Evapotranspiration

ETWatch

Energy balance

Validation

Hai Basin

Remote sensing

SUMMARY

The latent heat of evapotranspiration (ET) plays an important role for water resource management in water scarcity areas. Compared to the water balance method or to *in situ* measurements, an operational integrated monitoring method of regional surface ET from remote sensing data is a potentially useful approach to achieve water saving. This study presents new algorithms for the aerodynamic roughness length for complex landscape, for gap filling for cloud days, and for data fusion at different resolutions, based on the Penman–Monteith equation. It also presents an improved algorithm for ET calculation with remotely sensed data for clear days. Algorithms were integrated into the ETWatch. The research objective was to present the enhanced features of the ETWatch algorithm and its validation in the 320,000 km² Hai Basin in Northern China. This area faces serious over-exploitation of groundwater. ET was modeled and extensive field campaigns were done to collect data on soil moisture depletion, lysimeter measurements, eddy covariance measurements, and water balance calculations at diverse landscapes. The overall deviation for individual fields on a seasonal basis was 12% and decreased to 6% for an annual cycle. For larger areas, the deviation was 3% for an annual cycle. These levels of deviation are within the error bands for *in situ* measurements. The study concludes that data sets from ETWatch are able to aid consumptive water use reduction management in the study area.

© 2012 Elsevier B.V. All rights reserved.

1. Introduction

ET measurement requires advanced field instrumentation with a high level of data screening and interpretation. Typically, ET measurement techniques consist of lysimeters, surface renewal systems, heat pulse velocity, Bowen ratio systems, eddy covariance systems and large aperture scintillometers (e.g. Dugas et al., 1991; Meijninger and De Bruin, 2000; Castellví and Snyder, 2010). In addition, ET could be derived from soil moisture depletion profiles, which require buried moisture sensors and accurate measurements of irrigation water supply, along with estimates of recharge. While they can provide a reasonable measure of the local ET fluxes for relatively small areas, they are incapable of deriving ET fluxes across heterogeneous terrain, especially in mountainous areas. Recently, a new spatial ET tool was developed to estimate ET on an operational basis at the basin scale, which comprises a wide variety of ecosystems and landscape conditions (Wu et al., 2008).

Different tools exist to obtain ET values spatially. Kite and Droogers (1999) and Khan et al. (2010) summarized the capacity

of hydrological models, remote sensing algorithms, and field devices to describe its spatial distribution. Meteorological models used for weather forecasting and climate change have been coupled to Soil–Vegetation–Atmosphere–Transfer (SVAT) schemes (e.g. Chen et al., 1996). SVAT schemes have the capacity to model ET with grid sizes of typically 25–100 km. The advantage of numerical models is their ability to predict future situations, and to study the impact of interventions. They lack, however, detailed spatial information, as generally, the spatial resolution of numerical models covers tens of kilometers or even coarser.

Remotely sensed data, especially those from polar-orbiting satellites, provide us with temporally and spatially continuous information over land surfaces. They are useful for accurately parameterizing surface bio-physical variables, such as albedo, biome type and leaf area index. Current satellite approaches can accomplish a dynamic update of the actual surface flux state whenever the remote sensing data are available without precipitation and soil moisture as input. Instantaneous ET rates are thus linked to observables like land-surface temperature and vegetation cover fraction. Reviews of existing approaches are provided by Courault et al. (2005), Kalma et al. (2008) and Allen et al. (2010).

* Corresponding author. Tel.: +86 10 64855689; fax: +86 10 64858721.

E-mail address: wubf@irsa.ac.cn (B. Wu).

Identification and monitoring of ET for water planning and management requires an operational ET algorithm that is able to generate continuous ET data both at the field scale and at the basin scale. Wu et al. (2008) and Xiong et al. (2010a) developed ETWatch for monitoring spatial ET for operational purposes following models such as in Alexi and Disalexi (Norman et al., 1995a; Anderson et al., 1997), SEBS (Su, 2002) and SEBAL (Bastiaanssen et al., 2005). This was done by integrating the entire processing chain at both the field and basin scale environment. ETWatch has been intensively and independently verified, also by third parties, in various approaches across different fields and landscapes.

Many field measurement methods exist that can be used to validate remote-sensed ET products. The lack of flux evaluation standards, however, hinders effective validation. Farahani et al. (2007) pointed out in his review that the error between the Bowen ratio and an eddy correlation instrument is often up to 20%. For well-maintained and calibrated sites, this error can be reduced to 10% (Glenn et al., 2007), but it can also increase rapidly if the underlying heterogeneity increases. Li et al. (2005) performed a comprehensive evaluation of energy balance closure at the ChinaFLUX, finding that sensible heat and latent heat turbulent fluxes tend to be underestimated, and available energy may be overvalued. The disclosure of energy balance measures in AmeriFlux sites is summarized in Wilson et al. (2002). Although LAS measurements can be comparable to pixel-scale fluxes obtained with remote sensing, ground experiments show that the influence of source area and mixing height needs further study (Marx et al., 2008). Variability effects of the source area depend upon the choice of source area functions and also on: (i) height above the surface, (ii) wind speed, (iii) wind direction and (iv) surface roughness, amongst others. Wu et al. (2010) discussed the existence of source area models suggested by Schmid (1994), Gockede et al. (2005) and Kustas et al. (2006). These source area models have been considered in our comparison between remote sensing and field measurements described hereafter. Kalma et al. (2008) summarized 30 cases of flux validation in recent years, mainly based on EC systems, the Bowen ratio, and flux tower networks. The results showed that the accuracy of ET observations is influenced by many factors, including uncertainty in ground-based observations, the temporal-scaling algorithm and the source area. Effective methods still have not been developed to properly calculate some key parameters in the model, such as resistances or roughness length. Therefore, evaluation based on a water-balance equation at the watershed or sub-basin is a good optional (Wu et al., 2009, 2010).

Apparently, no single field measurement is perfect to validate ET monitoring results. For that reason, this study verified ETWatch

in the Hai Basin using a variety of methods, including field measurement, lysimeter, eddy covariance system, LAS, and the water balance of the sub-watershed at a different scale. The objective of this paper is to describe the ETWatch integration and improvements and to validate its performance at spatial scales ranging from the field, through the village, county, and sub-basin scale to the basin scale with diverse landscapes.

2. ETWatch

2.1. ETWatch structure

ETWatch has originally been developed as an operational software system for regional ET monitoring, on request of the Hai Basin commission (Wu et al., 2008, 2010; Xiong et al., 2010a,b). ETWatch consists of five subsystems and a system database (Fig. 1). The five subsystems include data acquisition, data pre-processing, ET monitoring, ET application, and database management system. An operational platform serves for the trained engineers to estimate ET themselves rather than by developers or specialized remote sensing/ET specialists. This is essential to sustainability of water planning and management. ETWatch has been customized for and deployed at the Haihe Basin Commission of Ministry of Water Resources and Beijing Municipal of Water Affair since 2008.

2.1.1. Data acquisition

The data acquisition subsystem is responsible for collecting MODIS, TM data, meteorological data and atmospheric boundary layer radio soundings data. Diurnal MODIS data can be downloaded from a VSAT (Very Small Aperture Terminal). Because of the high storage requirement (20–40 Gb daily), a timely data transmission is performed. The diurnal meteorological data and atmospheric boundary layer radio soundings data are shared by the meteorological data center of the National Meteorological Bureau.

2.1.2. Data pre-processing

According to the data types acquired by the data acquisition subsystem, the different processing methods and processes are developed. Pre-processing for remote sensing data includes radiometric, geometric and atmospheric corrections, cloud detection and land surface parameters calculation modules. The land surface parameters calculation module includes five key land surface parameters from multi-spectral radiances: land surface albedo, land surface temperature, spectral vegetation index, land surface emissivity, and surface roughness. The retrieval of remote sensing

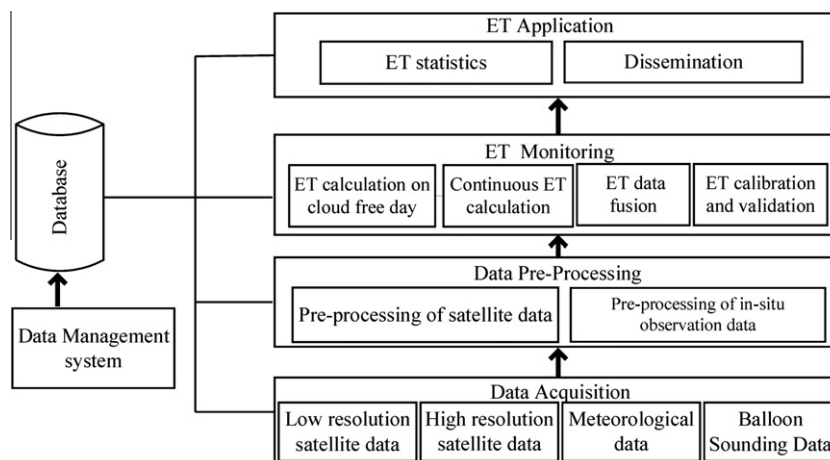


Fig. 1. ETWatch structure.

land surface parameters is not only affected by the satellite observation angle and atmospheric conditions, but also by the undulated land surface characteristics. In order to eliminate the impact of these physical conditions, ETWatch has embedded the 6S atmospheric radiative transfer model to conduct atmosphere corrections (Stein and Zaadnoordijk, 1999, Vermote et al., 1997). The consistency of the atmospherically corrected spectral reflectance data between various satellite overpass days has been greatly improved due to these standard correction procedures. The land surface temperature is retrieved by the split window algorithm proposed by Wan and Li (1997) and Mao et al. (2005), which eliminates the effects resulting from atmospheric water vapor on the transmittance of long wave radiation through the atmosphere.

Meteorological data processing comprises sunshine hours, air temperature, air pressure, air humidity and wind speed. *In situ* records were interpolated into daily map at 1 km resolution. Solar radiation was estimated with clear sky radiation and relative sunshine duration. Except sunshine duration, all variables above were corrected with elevation above sea level. The inverse distance squared method was commonly used for air temperatures and air pressure in combination with DEM data, whereas thin plate splines were employed for other variables (Qian et al., 2005). Approximate instantaneous maps of air temperature were calculated from daily maximum air temperature using a sine conversion.

2.1.3. ET monitoring

Multi-spectral radiance in the visible, near-infrared, thermal-infrared, and microwave region of the electromagnetic spectrum are combined with routine micro-meteorological ground data, atmospheric boundary layer radio soundings data, and digital elevation model data to describe the land surface fluxes. The ET monitoring subsystem consists of ET calculation on cloud-free day, continuous ET calculation, ET data fusion and ET calibration and validation modules. Details of the three ET calculation modules are described in Section 2.2. In ET calibration and validation module, several key input parameters are presented as follows.

- (1) The air temperature of the boundary layer is an important input. The inconsistency of observation time with satellite land surface temperature is usually ignored. Therefore, air temperature in the boundary layer (12:00 a.m.) was adjusted to the MODIS/Aqua transit time (13:30), assuming that the change of such air temperature is according to the sine function, as:

$$T_{12} - T_0 = A \sin\left(\frac{\pi}{2} \cdot \frac{3}{4}\right)$$

$$T_{13:30} - T_0 = \frac{A}{2} \sin\left(\frac{\pi}{2} \cdot \frac{3}{4}\right) + \frac{A}{2}$$
(1)

where *A* is the amplitude of daily air temperature.

- (2) The height of the mixed layer, the friction velocity, and the temperature gradient between land surface and atmosphere is determined by Brutsaert (1999) with daily Planetary Boundary Layer (PBL) measurements. The PBL record is obtained from seven different meteorological stations with weather balloons.

All parameters are calibrated by using local datasets based on independent parameter estimation software. An auto-calibration module is integrated into ETWatch. The PEST (Parameter Estimation) tool package was used for model parameter calibration and optimization in ETWatch. PEST, which is now widely applied to underground water and surface hydrological geology, geophysics, and chemistry, is a powerful independent parameter estimation procedure for model calibration based on the Gauss–Marquardt–Levenberg steepest descent algorithm (Marquardt, 1963).

Initialization values are calculated from local measurements. A PEST-based automatic calibration module integrated into ETWatch can be customized according to the remote sensing data, the underlying structure and the climatic regions. The calibrations were applied to LST estimation, the daily solar radiation (*R_{so}*) with flux site observation data, daily empirical relationship between *R_n* and *G₀* of the water body with pan evaporation data measured in the reservoirs, and aerodynamic resistance with LAS observations data at sites. Calibration is essential for the application of remote-sensed products (Xiong et al., 2011).

2.1.4. ET application

The ET application subsystem is developed to meet the requirement on different types of information dissemination from users. The subsystem consists of a statistical analysis of ET and of information dissemination modules. A grid based statistical analysis method provides water consumption results for different provinces and counties, for different land use types and for plots that are interesting to farmers and decision makers for water resource management.

Information dissemination aims to realize the query of historical and real-time ET monitoring results. The dynamical demonstration of the ET map with a color legend is developed under the support of the ArcIMS platform. ET statistical information of counties and different land use types are demonstrated by means of the temporal process change curves. ET of interesting plots can be calculated directly after a region is selected by the user.

2.2. Method

ETWatch is an integration of the “Residue Approach” and Penman–Monteith (P–M) (Fig. 2). The “Residue Approach,” i.e. the energy balance model, is computed from spectral radiances on cloud free days. The surface energy balance in simplified form reads as:

$$\lambda E + H = R_n - G_0$$
(2)

where *R_n* (*W m⁻²*) is the net radiation absorbed at the land surface, *G₀* (*W m⁻²*) the soil heat flux, *H* (*W m⁻²*) the sensible heat

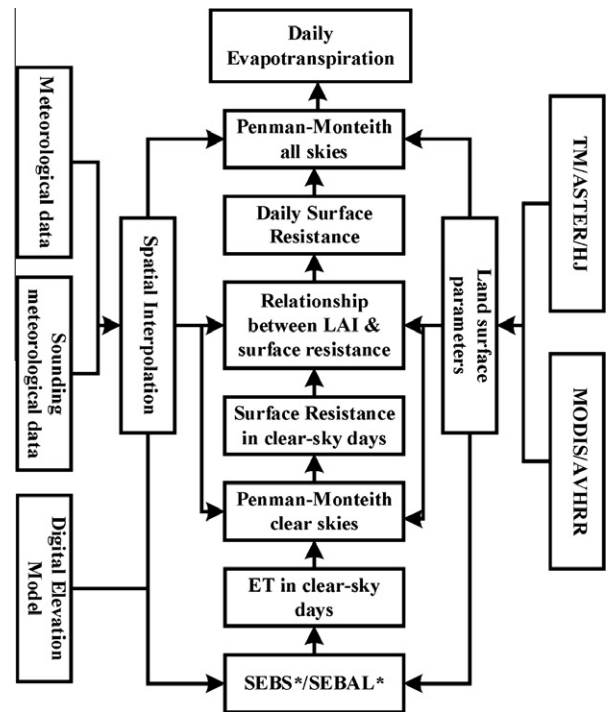


Fig. 2. Flowchart of the key procedures embedded in ETWatch (Wu et al., 2008).

flux and λE ($W m^{-2}$) the latent heat flux associated to evapotranspiration from water, soil, vegetation and other surfaces. The latent heat flux density ($W m^{-2}$) can be converted into actual ET rates ($mm d^{-1}$) using the temperature dependent latent heat of vaporization and the density of water. λE is computed as the residue of R_n , G_0 and H .

Existing energy balance models are modified and optimized independently before embedding into ETWatch, with a number of improvements and calibrations to handle the physical system of the Hai Basin. SEBS (Su, 2002) is improved to deal with moderate-resolution remote sensing data (1 km) for ET maps encompassing the entire basin. For the remote sensing data (30 m), the ETWatch adopts the calibrated and improved METRIC/SEBAL model (Allen et al., 2007; Bastiaanssen et al., 1998, 2005).

Due to cloud cover and satellite overpass interval, any ET dataset contains large temporal gaps. In the Hai Basin, for instance, MODIS provided on average 22% daily clear-sky coverage annually. An adequate solution for the intermittent period is based on the Penman–Monteith model (PM) described by Monteith (1965). It is used in ETWatch for inversion of surface resistance and calculation of daily ET data with intermittent remote sensing data to generate continuous ET data series under all sky conditions. This avoids the need for daily satellite data and diminishes the dependence of ETWatch on cloud free weather conditions.

2.2.1. Aerodynamic roughness length (z_{0m})

Transfer of momentum in aerodynamically rough air flows over a vegetated surface is primarily independent of molecular viscosity and is transferred to a large extent by pressure forces. The surface roughness affects the drag between land and atmosphere, and as a consequence also the exchange of momentum, heat and water vapor. Because surface roughness exhibits dynamic changes, z_{0m} must be derived from satellite observations for practical reasons (e.g. David et al., 2004). Three factors were taken into account to obtain the roughness length for momentum transfer z_{0m} . The roughness resulting from vegetation cover z_{0m}^v has been computed following Jia and Wang (1999):

$$z_{0m}^v = \left(NDVI \cdot \frac{1 + NDVI}{1 - NDVI} \right)^{1/2} \quad (3)$$

The roughness originating from topographical terrain variation has been included according to (Xiong et al., 2007):

$$z_{0m}^T = z_{0m}^v \cdot \left(\frac{slope - a}{b} \right) \quad (4)$$

The required *slope* data were determined from the 90 m SRTM digital elevation model that has been downloaded for the entire Hai Basin. The factors *a* and *b* are empirically determined coefficients (Xiong et al., 2007).

The aerodynamic roughness caused by non-vegetation obstacles (such as buildings, micro-terrain) was included for the roughness length for momentum transfer. A solution based on radar backscatter values is proposed (Zhu et al., 2002):

$$\log(z_{0m}^r) = -1.221 + 0.0906(\sigma_0) \quad (5)$$

where σ_0 represents the radar backscatter (dB) measured by the ASAR sensor aboard the ENVISAT satellite. The ASAR backscatter data is aggregated from 150 m to 1 km spatial resolution by simple areal averaging for compatibility with the MODIS thermal infrared data. The total term for surface roughness from integrating the three contributions is:

$$z_{0m} = \omega_1 \cdot z_{0m}^v + \omega_2 \cdot z_{0m}^T + \omega_3 \cdot z_{0m}^r \quad (6)$$

The weighing coefficients ω are determined as either 1.0, 1.0, and 0.25 using empirical fitted ways based on reference values given by Zhu et al. (2002, 2004). Heat transfer from a vegetated surface is primarily controlled by molecular diffusions whereas the Reynolds analogy with the transfer of moment does not apply. A correction term is needed for the surface roughness length for the heat transfer z_{0h} that is computed from the classical relationship proposed by Chamberlain (1966) and Thom (1972):

$$z_{0h} = z_{0m} / \exp(kB^{-1}) \quad (7)$$

The models for kB^{-1} proposed by Su et al. (2001) are included.

2.2.2. Gap-filling algorithm in cloudy days

Techniques for filling ET gaps between consecutive satellite data dates have been investigated to facilitate the determination of accumulated ET. The gap-filling procedure in SEBS is to apply the “self-preservation” character of the evaporative fraction (EF) from one clear day to several days (e.g. Shuttleworth et al., 1989; Crago and Brutsaert, 1996). The same theory is applied by SEBAL and METRIC to obtain accumulated ET with limited remote sensed observations (Allen et al., 2005), while ETWatch utilizes the Penman–Monteith method for time integration. The Penman–Monteith model was found adequate for estimating the magnitude of ET flux variations in temperate and tropical ecosystems, provided that the proper bio-physical parameters can be attached (Farah, 2001; Cleugh et al., 2007; Mu et al., 2007).

The surface resistance (r_s) in the Penman–Monteith equation, expressing the situation of soil moisture and vegetation stomata aperture, is computed on cloudfree days from the latent heat flux inversion. In ETWatch (Allen et al., 1998), the daily surface resistance ($r_{s,daily}$) is extended from r_s in neighboring cloud free days, smoothed LAI values, soil moisture content and the daily reductions functions for stomatal aperture response to minimum air temperature $m(T_{min})$ and vapor pressure deficit $m(VPD)$:

$$r_{s,daily} = \frac{r_{min,daily}}{LAI_{daily} \cdot SM_{daily}} = \frac{r_{min,clear} \times LAI_{clear} \times SM_{clear}}{LAI_{daily} \times m(T_{min}) \times m(VPD) \times SM_{daily}} \quad (8)$$

where $r_{min,daily}$ is the daily bulk stomatal resistance of the well-illuminated leaf, LAI_{daily} is a daily dataset of Leaf Area Index (LAI) values being smoothed by a Savitzky–Golay filter (Chen et al., 2004), and SM_{daily} is the daily soil moisture content retrieved from AMSR-E microwave brightness temperature (Gruhier et al., 2008). Further, $r_{min,clear}$ is the bulk stomatal resistance of the well-illuminated leaf on the clear-day, LAI_{clear} is LAI calculated using clear-day satellite data and SM_{clear} is the soil moisture content retrieved from AMSR-E on the clear-day.

2.2.3. Data fusion of different resolution data

Due to cloud restrictions and satellite overpass interval, there were insufficient high resolution data available for regular processing of ET data with 30 m pixel resolution throughout the year. HJ satellite data are only available since 2008. Hence the historical studies were undertaken with Landsat and ASTER. Computation of seasonal and annually accumulated ET values with 30 m pixels was done by a data fusion technique between 1 km (AVHRR/MODIS) and 30 m (Landsat/ASTER) based ET data. The accumulated ET values for any period were computed at the MODIS pixel resolution. Subsequently, the accumulated MODIS-based ET data at the 1 km resolution were downscaled using Landsat-based ET data on particular dates that provided proper representations for the periods. The STARFM model was used (Gao et al., 2006) that is based on a moving window technique for minimizing the effect of pixel outliers. The values of the center pixels were computed from the spatially and spectrally weighted mean difference of pixels within that particular window area:

$$L(x_{w/2}, y_{w/2}, t_2) = \sum_{i=1}^w \times \sum_{j=1}^w W_{ij} (M(x_i, y_j, t_2) + L(x_i, y_j, t_1) - M(x_i, y_j, t_1)) \tag{9}$$

where $L(x_{w/2}, y_{w/2}, t_2)$ is the ET of a Landsat pixel predicted for time t_2 , $L(x_i, y_i, t_1)$ is the calculated ET of a Landsat pixel for time t_1 , W is the size of the moving window, $x_{w/2}$ and $y_{w/2}$ are the center pixels within the moving window and $M(x_i, y_i, t_1)$ and $M(x_i, y_i, t_2)$ represent the ET calculated from MODIS images at t_1 and t_2 , respectively.

The advantage of STARFM is to keep a good consistency between MODIS pixel and fused result (Liu et al., 2011a). The histogram of the fused data combines the spatial patterns of 1 km data with the 30 m data. The trend of the histogram is consistent with the 1 km ET data, which shows that the results preserve the temporal character of low-resolution ET data. Fused data are well-correlated with the high-resolution ET data at Landsat pixel resolution.

3. Validation sites and methods

The Hai Basin (~320,000 km²) is located on the North China Plain and the Basin encompasses both the alluvial plain the adjacent mountains. The alluvial plain consists of a composite of various rivers that flow parallel from the mountains in the West to the Bohai Sea in the East (see Fig. 3). The average annual rainfall across the basin between 1980 and 2005 was 498 mm yr⁻¹, according to the water resources bulletins of the Hai Basin. Total actual evapotranspiration (ET) of all land surface types (e.g. crops, forests, lakes and urban areas) for 8 yr was 542 mm yr⁻¹. The aquifer system augments the shortage of surface water during the dry season to meet the demand of water borne economies, including irrigation, industries, ports and fishponds. Due to an over-exploitation, the groundwater table in the alluvial plain is

declining at a rate of 1–5 m yr⁻¹ (Liu et al., 2001; Foster et al., 2004). This trend can be curtailed by reducing the basin-wide ET (Bastiaanssen et al., 2008). Reductions in ET will also restore catchment water balances, ecosystem functions, and increase outflow to the Bohai Sea. River basin agencies, however, rarely consider ET reduction as an option for water resource management. An exception in this respect is the Hai Basin Commission’s proposal for evapotranspiration reduction. One of the vital reasons is the lack of spatially distributed reliable ET data for assessments of consumptive water use at local scale.

Validation has been implemented in the Hai Basin of China using a variety of methods because of the complex terrain of Hai Basin, including field measurement, lysimeter, eddy covariance system, LAS, and the water balance of the sub-watershed at a different scale (Table 1). Soil moisture depletion measurements provide a local measurement of water withdrawals that can be ascribed to ET rates, after correction for percolation losses. Lysimeter measurements with an area of 1m² indicate the changes in weight of only a small fraction of the 30 m pixel. Lysimeter measurements however are useful only if the measurements represent one or more pixels (e.g. Allen et al., 2005). The Eddy Covariance (EC) and the Large Aperture Scintillometer (LAS) measure the turbulent ET fluxes at a specific height above the land surface. The LAS has been used to measure average sensible heat flux from 200 m to 10 km (McAneney et al., 1995).

Soil moisture depletion was conducted at Guantao County in the Hai Basin. This county is actively involved in water conservation practices, and the water managers are highly motivated to reduce ET. Soil moisture dynamics have been measured *in situ* on fields with maize, wheat, and cotton near the towns of Beidonggu, Shilidian, and Nanyulin during 2005. The measurements were carried out by local people for executing the World Bank water conservative project. Specifications of the sites and crop types as well as the measurements are provided in Table 2. The calculation of ET is based on soil water balance equation.

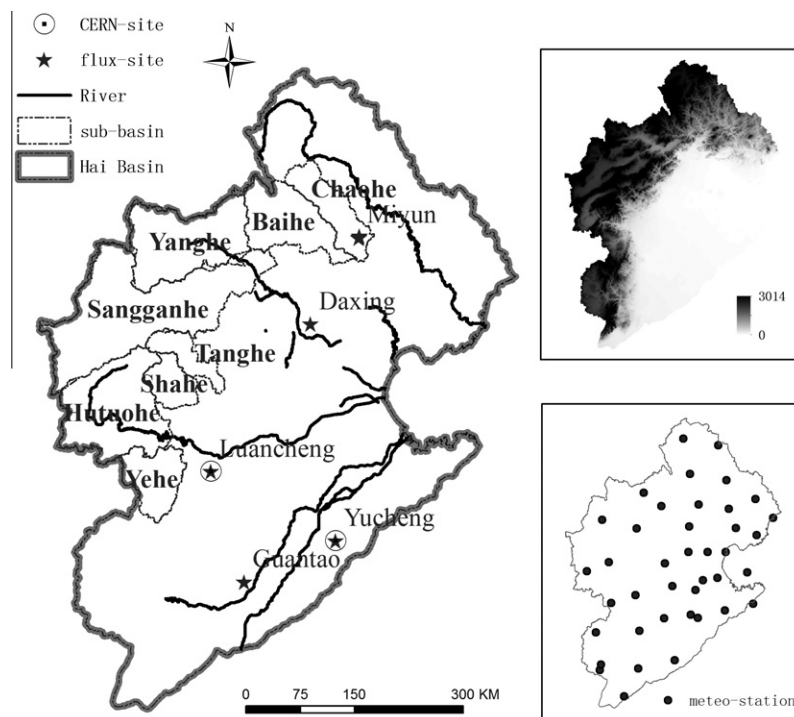


Fig. 3. Location of the Hai Basin on the North China Plain (The left map is subbasin in Hai Basin, the upright map is DEM of the Hai Basin and the down map is meteorological station).

Table 1
Different spatial scales incorporated in the validation of remotely sensed ET maps.

Measurement technique	Spatial scale (m)	Pixel size
Soil moisture depletion	0.3	Thematic mapper
Lysimeter	1	Thematic mapper
Eddy co-variance (EC)	1000	Thematic mapper; MODIS
Large aperture scintillometer	5000	Thematic mapper; MODIS
Watersheds	10,000	Thematic mapper; MODIS
Sub-basin	100,000	MODIS
River basin	400,000	MODIS

The Institute of Geography Science and Natural Resources Research (IGSNRR) of Chinese Academy of Sciences has an ongoing lysimeter study at Yucheng County in Shandong Province, also located in the Hai Basin. A lysimeter is used to measure the amount of actual evapotranspiration released by plants. By recording the amount of precipitation that an area receives and the amount lost through the soil, the amount of water lost to evapotranspiration can be calculated (Vaughan et al., 2007). The lysimeter is located at 116.6°E Longitude and 36.95°N Latitude (Fig. 3). The weighing lysimeter was cropped with a traditional wheat–maize rotation scheme. The lysimeter of a dimension of 1 m length × 1 m width × 2.4 m depth was located in the middle of a 6.25 ha field. The monthly lysimeter measurements are provided in Table 3.

The Hai Basin also hosts two flux sites as part of the China Flux network that is maintained by the Chinese Ecosystem Research Network (see Table 4 and Fig. 3) (<http://www.chinaflux.org/en/index/index.asp>). The flux data were collected and cleaned for comparison against ETWatch modeling results. For the sake of standardization, the China Flux sites were equipped with similar instrumentation. The sites have an EC system for latent heat and CO₂ fluxes at a height of 2.10 m above the winter wheat land surface. The devices were mounted 3.30 m above the ground for the maize crop. Average values were calculated and recorded every 30 min. A net radiometer (CNR1, Kipp & Zonen, Delft, The Netherlands) was installed at a height of 2.10 m in winter wheat and 3.30 m in summer maize to measure incoming, reflected, and emitted components of shortwave and long wave radiation. Air temperature and relative humidity were measured with a temperature/humidity probe (HMP45C, Vaisala, Helsinki, Finland). Wind speed was measured with an anemometer (A100R, Vector Instruments, Rhyll, United Kingdom). Two soil heat flux plates (HFPO1SC, Hukseflux, Delft, The Netherlands) were

Table 3
Lysimeter with wheat–maize crop rotation, Yucheng, Year 2003.

Month	Lysimeter (mm)	ETWatch (mm)	Deviation
January	17	8	–53%
February	25	20	–20%
March	44	48	9%
April	128	131	2%
May	203	148	–27%
June	77	70	–9%
July	92	101	10%
August	125	129	3%
September	87	94	8%
October	49	28	–43%
November	23	11	–52%
December	10	11	10%
Total	880	799	–9%

installed at 0.10 m below the soil surface within and between rows. The EdiRe software (University of Edinburgh, <http://www.geos.ed.ac.uk/abs/research/micromet/EdiRe>) was used to process the EC data, including spike detection, lag correction of H₂O/CO₂ relative to the vertical wind component, sonic virtual temperature correction, coordinating rotation using the planar fit method, corrections for density fluctuation (WPL-correction), and frequency response correction, etc. (Liu et al., 2011b).

The GEF Hai Basin project provided the necessary funds to support existent and new field sites for the independent validation of the ETWatch algorithm results (Table 4). The three sites have equipped LAS systems for heat flux, a net radiometer for net radiation, and two soil heat flux plates. Pre-processing of LAS data is complex, as it includes quality control of observational data, calculation of the temperature structure parameter, a stability correction, calculation of the friction velocity and the sensible heat flux and gap-filling of missing data (Liu et al., 2011b). The soil surface heat flux was derived by the temperature prediction-correction method (Yang and Wang, 2008).

Turbulent fluxes obtained from the EC and LAS measurements reflect the influence of the underlying surface on the turbulent exchange (Schmid, 2002). The source area of the EC and LAS measurements should be determined before validation. An Eulerian analytic flux footprint model (Kormann and Meixner, 2001) was used to obtain the flux of a single point vertical flux measurement. For the LAS flux observations, the path-weighting function of the LAS (Meijninger et al., 2002) was combined with the above point flux footprint model. The monthly flux source area of the EC and

Table 2
Specifications of soil moisture depletion measurements in the Guantao County (2005) (Fc: the fractional canopy coverage).

ID	Name	Longitude	Latitude	Land use	Fc (%)	Field ET(mm)	ETWatch (mm)	Deviation (%)
1	Shilidian	115.369 E	36.706 N	Wheat	86	324	345	6
2	Shilidian	115.365 E	36.708 N	Wheat	48	326	392	20
1	Shilidian	115.369 E	36.706 N	Maize	77	332	313	–6
12	Shilidian	115.369 E	36.708 N	Maize	65	353	310	–12
19	Shilidian	115.381 E	36.708 N	Cotton	63	408	440	8
6	Shilidian	115.378 E	36.706 N	Cotton	44	495	578	17
7	Beidonggu	115.255 E	36.608 N	Wheat	46	328	415	27
8	Beidonggu	115.250 E	36.609 N	Wheat	47	335	416	24
9	Beidonggu	115.255 E	36.608 N	Wheat	58	353	304	–14
6	Beidonggu	115.255 E	36.609 N	Maize	38	353	260	–26
7	Beidonggu	115.255 E	36.608 N	Maize	77	370	373	1
8	Beidonggu	115.250 E	36.609 N	Maize	43	405	302	–25
9	Beidonggu	115.255 E	36.608 N	Maize	40	520	680	31
24	Beidonggu	115.254 E	36.609 N	Cotton	76	545	565	4
4	Nanyuning	115.393 E	36.704 N	Maize	88	334	329	–1
5	Nanyuling	115.396 E	36.703 N	Wheat	78	341	315	–8
3	Nanyuling	115.399 E	36.705 N	Wheat	86	370	392	6
4	Nanyuling	115.393 E	36.704 N	Wheat	50	425	365	–14
20	Nanyuling	115.400 E	36.704 N	Cotton	48	552	622	13
21	Nanyuling	115.384 E	36.705 N	Cotton	54	553	609	10

Table 4

Location of the eddy covariance sites under auspices of the Chinese Ecosystem Research Network (CERN) as part of Asia Flux and sites for the Global Environmental Facility (GEF) network.

Location	Project	Landscape	Land use	Coordinates	Period of measurements
Yucheng	CERN	Plain	Wheat, maize	39.95 N; 116.6 E	2006 and 2007
Luacheng	CERN	Plain	Wheat, maize	37.88 N; 114.68 E	2007 and 2008
Daxing	GEF	Sub-urban	Wheat, maize	39.61N; 116.43 E	2005 and 2006
Miyun	GEF	Mountain	Fruit trees	40.63 N; 117.32 E	2006 and 2007
Guantao	GEF	Plain	Wheat, maize	36.515 N; 115.126 E	2006 and 2007
Xiaotangshan	BNU	Sub-urban	Bare, grass	40.183 N; 116.433 E	2004 and 2005

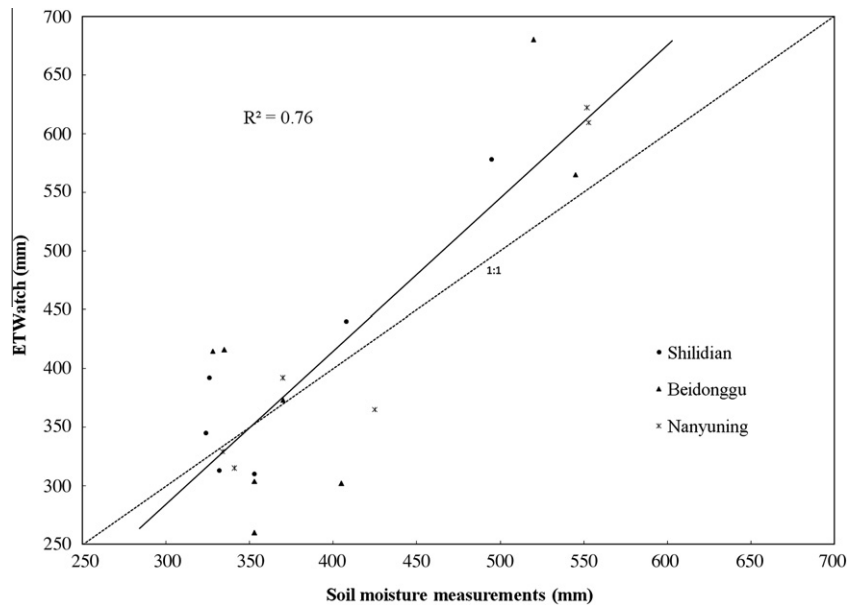


Fig. 4. ET derived from soil moisture depletion curves in Guantao County during 2005.

LAS flux measurements was obtained by averaging every half-hourly footprint when the sensible heat fluxes were larger than zero. Average ET value at an area of $3 \text{ km} \times 3 \text{ km}$ around EC the measurement point for 30 m resolution ET data from ETWatch was used for validation against the EC value, and the ET value at the central part of the LAS optical path was used for validation of 1 km ET data from ETWatch (Liu et al., 2011b).

Rainfall and discharge from eight small catchments were used as well to estimate ET at the sub-basin scale using the classical water balance method. The catchments of Yehe, Hutuo, Yanghe, Sanggan, Chaohe, Baihe, Shahe, and Tanghe rivers were used for this purpose (Fig. 3). Shashe (3770 km^2) is the smallest and Sanggan ($17,744 \text{ km}^2$) the largest catchment. These catchments are all located on the western side of the Hai Basin. This part of the study area includes mountainous catchments covered mostly with forests and grasslands. In eight catchments, average annual precipitation is calculated by using daily observations from 25 evenly distributed meteorological stations, and average annual runoff is calculated from eight hydrological gauge stations. The multi-year average change of soil water storage can be negligible. The average annual ET is the difference of precipitation and runoff based on the water balance equation (Yang and Fei Tian, 2009), which was used to compare ET from ETWatch.

4. Validation results

4.1. Soil moisture depletion

Soil moisture depletion was measured at 10 different combination of locations (Beidonggu, Shilidian, Nanyuling) and crop types

(wheat, maize, cotton) in Guantao County. The overall correlation between field measurements and ETWatch was high ($R^2 = 0.88$; $n = 20$) during 2005 (see Fig 4 and Table 2). The Root Mean Square Error was $16 \text{ mm season}^{-1}$ and the average relative error for an individual field was 13.6%. ETWatch estimates were only 4% higher if all 20 fields were grouped and considered as being a single village with a composite of agricultural fields. Hence, the seasonal ET of a composite irrigated cropland is slightly over-estimated by ETWatch.

For the six sites in Shilidian, the average ET was 373 mm as measured in the field, whereas ETWatch predicted 396 mm, i.e., a deviation of 6.3%. Measured soil moisture for Beidonggu was 401 mm, whereas the ETWatch estimate was 414 mm, i.e., a deviation of 3.3%. ETWatch best performed in Nanyuning (2.2% deviation): ET with field measurements was 429 mm and ETWatch predicted 439 mm. The higher ET values in Nanyuning reflect the higher fraction of cotton fields in the dataset.

If ET data are grouped based on vegetation coverage, the deviation has a strong relationship with vegetation coverage. Therefore, a lower deviation occurs if fields have a homogenous, high vegetation cover, corresponding to a high matching of pixel data with field measurements (see Table 2).

4.2. Lysimeters

The results of the lysimeter measurements of the wheat-maize cycle in Yucheng Country are displayed in Fig. 5. Until DOY 127, the agreement is good, except for a few days with extreme high ET fluxes ($>10 \text{ mm d}^{-1}$) measured by the lysimeter. This is the cold period when winter wheat is the predominant crop. Higher

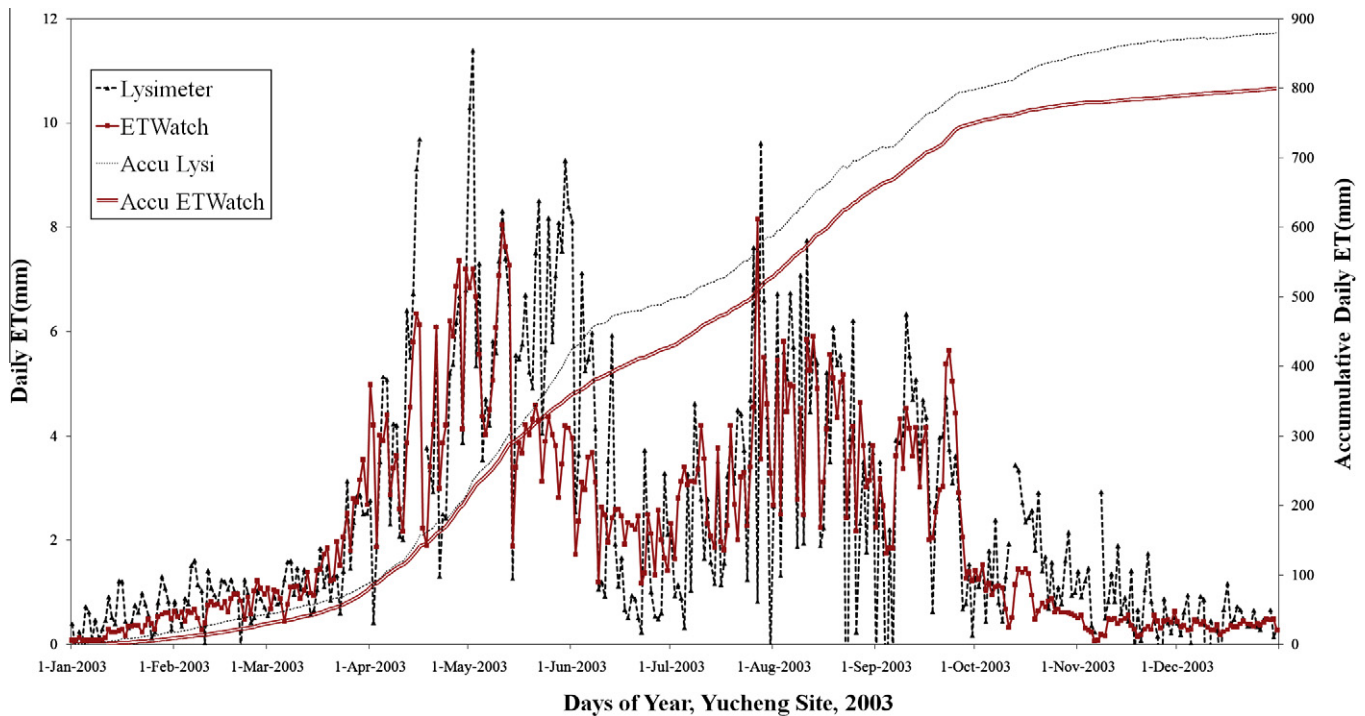


Fig. 5. Lysimeter measurements in a wheat-maize crop rotation at Yucheng during 2003. The accumulated values are also provided.

deviations occurred during the irrigation season of May 2003. The lysimeter produced exceptionally high ET values in the period between DOYs 127 and 163. It is unclear whether this deviation is related to (i) scale matching of lysimeters to the pixel at 30 m or 1 km, (ii) abundant irrigation supply, (iii) parameterization of ETWatch, (iv) non-availability of Thematic Mapper images during this period of the year, or (v) non-representation of local conditions in the lysimeter.

ET for the wheat season between October 1st and June 30st was estimated by ETWatch as 477 mm with rainfall of 232.1 mm during the season, and as 576 mm by the lysimeter. Apparently, the Yucheng lysimeter provided an over-estimation of the actual ET values as compared to other measurements. (Shen and Yang, 1998) gives a total ET for the full growing season of 480 mm for winter wheat when rainfall is 282 mm. A review of several articles on ET for wheat and maize in the Hai Basin was undertaken by Soppe et al. (2004) and Zhang et al. (2002, 2004a,b). They reported an average ET for wheat of 440 mm with values ranging between 250 and 485 mm. The values of Soppe (440 mm) and Shen (480 mm) Shen et al. (2004) agree with the observations of ETWatch (477 mm).

After DOY 170 the agreement improved, and this period coincides with the growth of the maize crop (Fig. 5). ET for the maize season between July 1st to September 30th was estimated by ETWatch as 324 mm and with the lysimeter as 304 mm, i.e. showing a 6.6% deviation. During the maize growing season, no irrigation was observed by the lysimeter. Comparing lysimeter readings with an ET value of 312 mm from neighboring pure pixels with maize coverage larger than 70%, we note a reduction in the deviation from 6.6% to 2.6%. These results show that ETWatch performs better in maize than in wheat and predicts a 9% lower ET for the annual cycle of 365 days (see Table 3).

4.3. Eddy covariance

The advantage of Eddy Covariance (EC) systems is that the latent heat flux is measured directly without involving water balance measurements (rainfall, irrigation, drainage, surface runoff, change

in storage) or energy balance measurements (net radiation, sensible heat flux, soil heat flux). The essential shortcoming of EC is the lack of energy balance closure (Norman et al., 1995b; Wilson et al., 2002).

EC data are fragmented due to weather condition, uncertainty and data sharing difficulties. Before 2006, only a few sites were located in the study area and EC had not been measured. We used CERN measurements to validate the results. Fig. 6 and Table 5 show the validation results for the latent heat flux. A high correlation ($R^2 = 0.91$) was observed at the Xiaotangshan (Beijing) site within the sub-urban landscape. The results of a few individual days in May and June are demonstrated. The total ET for 10 days measured by the EC system in a sub-urban environment was 19.94 mm, whereas ETWatch predicted 19.21 mm, i.e. a difference of 3.66% over a period of 10 days. The daily absolute average ET deviation was equal to 8.71%, being a common deviation for EC systems, whereas 2 days had an error larger than 15%. This shows

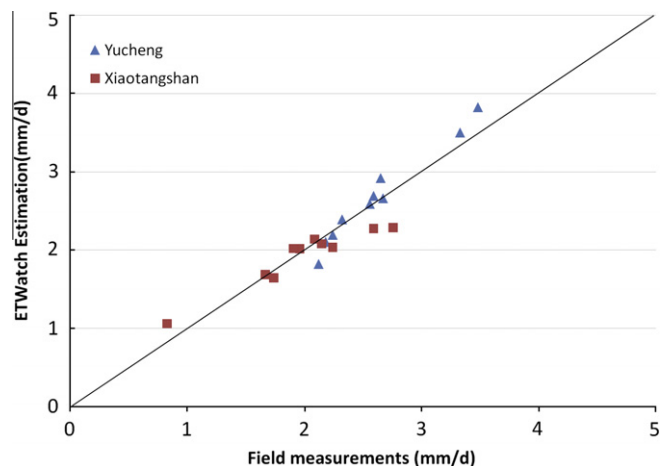
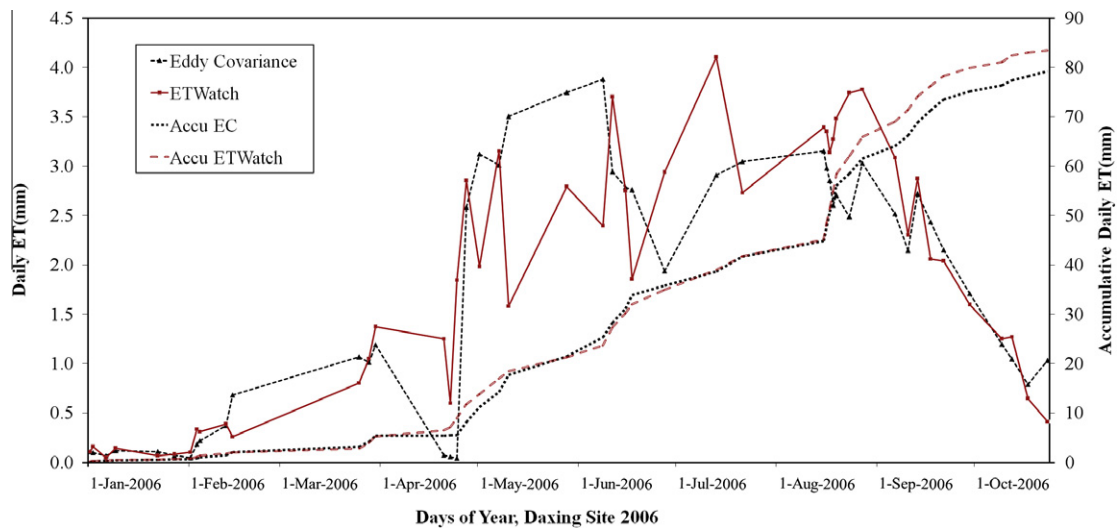


Fig. 6. ET measurements at the Xiaotangshan site (2004 and 2005) combined with the Yucheng data (2003).

Table 5

Eddy covariance measurements of latent heat flux. Source: advances in water science.

Sites	Date	With Modis	ECobs (mm)	ETWatch (mm)	Deviation (%)	Net radiation ((W m^{-2}))
Yucheng	May 20th (2003)		2.56	2.59	1.17	
Yucheng	May 21st (2003)		3.33	3.5	5.11	
Yucheng	May 22nd (2003)		3.48	3.82	9.77	
Yucheng	May 24th (2003)		2.12	1.82	-14.15	
Yucheng	May 25th (2003)	Y	2.67	2.66	-0.37	
Yucheng	May 26th (2003)		2.24	2.19	-2.23	
Yucheng	May 27th (2003)	Y	2.59	2.69	3.86	
Yucheng	May 28th (2003)		2.32	2.39	3.02	
Yucheng	May 29th (2003)		2.65	2.92	10.19	
Yucheng	May 30 (2003)	Y	2.18	2.1	-3.67	
			26.14	26.68	2.07	
Xiaotanshan	June 8th (2004)		1.74	1.64	-5.75	124.4
Xiaotanshan	June 9th (2004)	Y	2.09	2.14	2.39	148.1
Xiaotanshan	June 10th (2004)		1.96	2.01	2.55	141.1
Xiaotanshan	June 11th (2004)		2.15	2.08	-3.26	134.5
Xiaotanshan	June 12th (2004)	Y	1.67	1.68	0.60	112.5
Xiaotanshan	May 6th (2005)	Y/TM	2.59	2.27	-12.36	158.8
Xiaotanshan	May 7th (2005)		2.76	2.28	-17.39	143.6
Xiaotanshan	May 8th (2005)		1.91	2.02	5.76	97.8
Xiaotanshan	May 9th (2005)	Y	2.24	2.03	-9.38	143.8
Xiaotanshan	May 10th (2005)		0.83	1.06	27.71	34.8
			19.94	19.21	-3.66	

**Fig. 7.** Comparison of ETWatch against the EC-based ET fluxes in Daxing.

that the new parameterization of roughness for sub-urban areas contributed to a higher correlation. The same graph shows the validation against the EC measurements at the Yucheng (Shandong) site within the plain landscape. The total ET for 10 days EC measurements during May (2003) was 26.14 mm, whereas ETWatch provided a value of 26.68 mm for the same period, i.e. a deviation of 2.07%. On a daily time step, the absolute average deviation was 5.35%, and no day had an error larger than 15%. Comparing the two sites, we note that the sub-urban landscape site had a larger deviation. Average ETWatch deviation at satellite dates equals 4.61%, and is thus less than 7.36% of the average deviation at non-satellite dates. This means that the absence of satellite data contributes to approximately 60% deviation.

ETWatch results matched well with the accumulated ET for the two EC data sets at the Yucheng (Shandong) and Xiaotanshan (Beijing) sites. It can thus be concluded that bias is absent in ETWatch, and that ETWatch can be applied to different land use classes or landscapes. At Miyun County, an accumulated ET of 220 mm is measured by EC devices, whereas 222 mm is estimated by

ETWatch. This is an encouraging agreement and a confirmation that ETWatch predictions and EC correlate well.

The results of the Daxing site are presented in Fig. 7. Deviations on single days can be significant, but the correlation of the overall trends was high. The measured accumulated ET value for Daxing was 790 mm, whereas ETWatch provided a value of 815 mm (3% deviation). The onset of the difference in the accumulated ET values occurred during the second part of August 2006, which may due to the quality of the input images in rainy season.

A comprehensive EC data set was generated from the Chinese Ecosystem Research Network and GEF funded sites. Fig. 8 shows the scatter diagrams of the evaporative fraction from China Flux. The Luancheng site exhibited the highest correlation ($R^2 = 0.79$), and the evaporative fraction was typically over-estimated by 6%. The Yucheng site showed a highest data density with results that were close to the 1:1 line and a high correlation ($R^2 = 0.74$). The orchards in Miyun County had a similar correlation ($R^2 = 0.73$). The correlation in Daxing County was still high ($R^2 = 0.64$) whereas the regression line deviated somewhat more from the 1:1 line. In

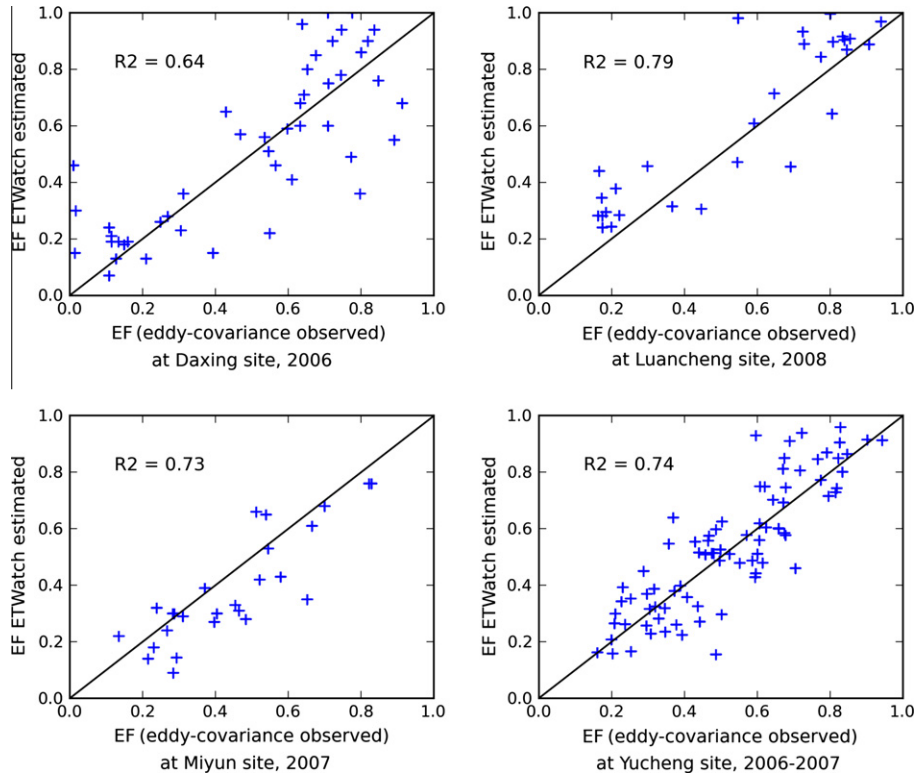


Fig. 8. Eddy covariance measurements of the Chinese Ecosystem Research Network during 2006 and 2007 and GEF funded sites.

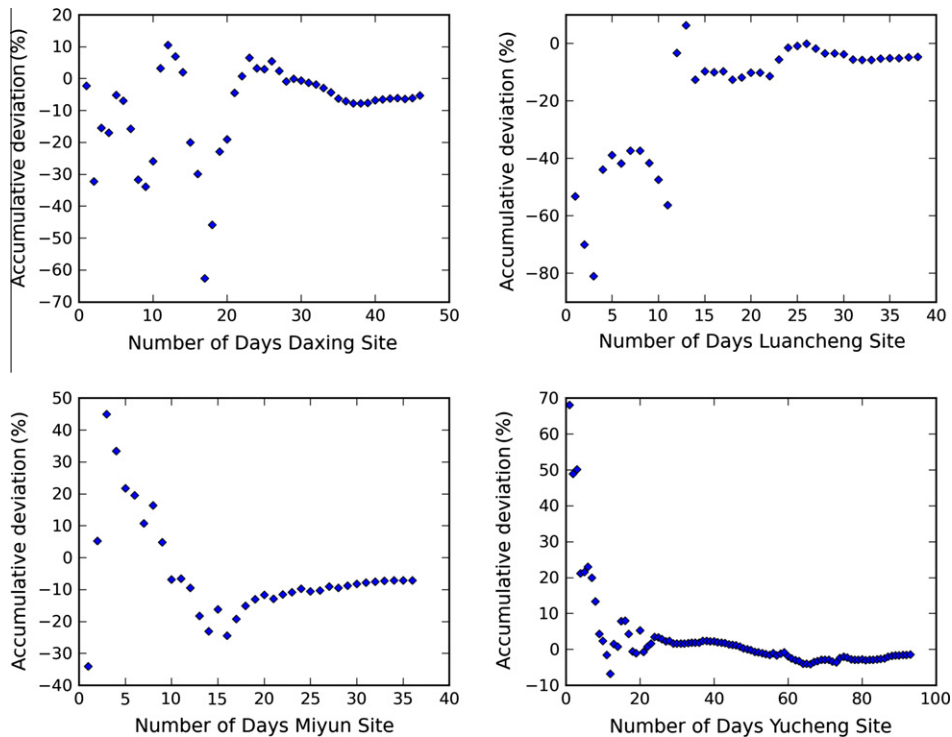


Fig. 9. Deviations between EC fluxes and ETWatch predictions over different time periods.

total, we conclude that ETWatch well performed in wheat-maize rotations and no systematic over-estimation or under-estimation of ETWatch could be detected. The deviations presented in Fig. 8 are non-systematic and occurred at all ranges of soil moisture and at four different sites with different landscapes, dispersed over

the Hai Basin. But the sub-urban site at Daxing had a larger deviation than the sites at plain and mountainous landscapes.

The effect of time integration on ET fluxes was further investigated by computing the deviations at different time scales. Variable time periods between 1 and 40 days were considered

Table 6
Water balance measurements of watersheds (data source: Yang et al., 2009).

	Area (km ²)	Rainfall (mm yr ⁻¹)	Runoff (mm yr ⁻¹)	Water balance ET (mm yr ⁻¹)	ETWatch (mm yr ⁻¹)	Deviation (%)
Shahe	3770	508	72	436	427	2.1
Tanghe	4420	451	62	390	402	-3.0
Yehe	6420	507	75	432	471	-8.3
Chaohe	6531	478	38	440	520	-15.4
Baihe	9945	454	10	444	459	-3.3
Yanghe	14,600	386	25	362	349	3.7
Hutuo	15,580	477	41	436	373	16.9
Sanggan	17,744	396	23	374	337	11.0

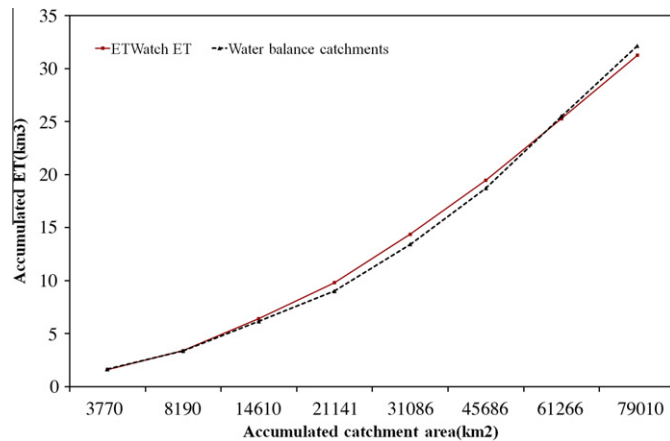


Fig. 10. Comparison of ET volumes estimated by ETWatch and by field measurements of the water balance (data source: Yang and Fei Tian, 2009).

(Fig. 9). The site at Daxing, located within sub-urban landscapes, displayed the largest deviations: 30% for a 40 day period. Because the other 3 EC flux sites did not have such a large deviation, this pointed to a systematic problem with the sonic anemometer or the infrared gas analyzer. The Luancheng site showed a deviation of 10%, which is within the generally acceptable range of EC flux accuracy. The Miyun site showed deviations of less than 10% for 20 days or longer, and the Yucheng site had the same performance. Apparently, half-month ETWatch values are accurate and within the margin of errors normally associated to EC flux measurements. Half-month time steps are commonly applied in water conservation practices and thus it is feasible to use ETWatch result for ET reduction management. Again, the sub-urban site has a larger uncertainty on ET estimation as compared to other sites.

Independent validation of ETWatch based on observation data is undertaken by researchers in Beijing Normal University, integrating it with the flux footprint model at different temporal scales (monthly/half-monthly and daily) and spatial resolutions (30 m, 1 km). Ground measurements from EC, LAS and AWS at Guantao, Daxing, and Miyun sites in the Hai River Basin were used, and rigorous data processing and quality control were executed as well (Liu, 2010). For monthly ET estimations at the Guantao site between 2007 and 2009, the Mean Relative Error (MRE) and the Mean Absolute Percentage Error (MAPE) of 30 m monthly ET as compared to the EC data were equal to -13.62% and 21.22%, respectively. The MRE of 1 km monthly ET was equal to 8.57%, and the MAPE to 19.46% as compared with LAS data. Since ETWatch data was consistent between 30 m and 1 km ET data, we conclude that EC was over-estimated and LAS was underestimated as compared to ETWatch. In addition, a good agreement between ETWatch values and ground measurements was found, with correlation coefficients above 0.90.

4.4. Catchment scale water balance

Validation of the ETWatch model performance at a larger scale was accomplished by comparing it to the water balance of small catchments. Water balance data were collected for the period between 2002 and 2005 (Table 6). The ET volume for each catchment was first compared, followed by an area integration of all catchments. The smallest catchment (Shahe) covers an area of 3770 km², whereas all catchments together cover an area of 70,910 km², approximately 25% of the total area of the Hai Basin. All catchments are located at the mountainous area at the western part of the Hai Basin.

The overall deviation was remarkably small because of the balancing out of individual high and low ET deviations. The maximum under-estimation of ET appeared to be -15.4% and occurred in the Chaohe sub-basin. The maximum over-estimation was +16.9% and occurred in the Hutuo sub-basin. Fig. 10 displays ET values according to the water balance measurements and ETWatch calculations as a function of increasing catchment area. This showed a difference of 2.4% as ETWatch estimated a total ET of 31.3 km³ yr⁻¹ and the water balance measurements showed a value of 32.1 km³ yr⁻¹.

The average annual ET for the entire Hai Basin according to ETWatch was 542 mm yr⁻¹ (2002–2005) which for an area of 320,000 km² is equal to 173.4 km³ yr⁻¹. ET estimates according to the water balance for the entire Hai Basin was 170.2 km³ yr⁻¹ or an equivalent amount of 532 mm (Zhang personal communication 2009). This is a difference of 1.8% and in the same ballpark as shown in Fig. 10.

4.5. Validation summary

ETWatch is a complicated computational model, including pre-processing of remote sensing data and meteorological data, quality control, data analysis, and assessment of realistic values. The accuracy of the results is subject to many factors. For example, satellite data availability is a prime concern due to frequent presence of clouds in the Hai Basin. Despite the complexity, it is the only method to produce ET data operationally for water management.

Table 7 summarizes the results of the data sets which were analyzed. It demonstrates that the annual ET data were more reliable

Table 7
Synthesis of the absolute deviations between field measurements and ETWatch calculations for the Hai Basin. Not all combinations had available datasets.

Spatial scale	Technique	Daily (%)	Season (%)	Annual (%)
Field scale	Soil moisture	N/A	13.6	N/A
Field scale	Lysimeter	N/A	11.3	9.0
Field scale	Eddy covariance	7.6	N/A	3.0
Village scale	Soil moisture	N/A	3.9	N/A
County scale	Soil moisture	N/A	3.7	N/A
Sub-basin scale	Water balance	N/A	N/A	3.8
Basin scale	Water balance	N/A	N/A	1.8

Table 8
Synthesis of the absolute deviations between field measurements and ETWatch calculations for the Hai Basin in different landscapes.

Landscape	Sites	Technique	Daily (%)	Month (%)	Annual (%)
Plain	Guantao	Eddy covariance	−5.72	4.49	N/A
		Large aperture scintillometer	−4.68	11.79	N/A
		Soil moisture depletion	N/A	N/A	4.00
	Luancheng	Eddy covariance	−17.70	7.41	N/A
	Yucheng	Eddy covariance	15.40	6.50	N/A
Sub-urban	Daxing	Eddy covariance	−13.72	−12.69	N/A
		Large aperture scintillometer	−2.20	4.31	N/A
	Xiaotangshan	Eddy covariance	2.60	N/A	N/A
Mountain	Miyun	Eddy covariance	N/A	−19.58	N/A
		Large aperture scintillometer	1.15	8.41	N/A
	Watersheds in the West	Water balance	N/A	N/A	3.80

than the daily ET data. The best performance was obtained at the basin scale with a deviation of 1.8%. Thus the overall basin ET data were more reliable than those of a single pixel or pitch. A lower agreement at the field scale was still acceptable for water conservation and ET reduction interventions, especially at time periods of a half-month or longer (see Fig. 9). The low frequency of high resolution Landsat images is a likely cause of a lower accuracy of ET measurements at the field scale. It is thus not related to the methodology, but to cloud cover and the long intermittence between consecutive high resolution thermal images. Appearance of new data source (HJ-1B, Landsat Data Continuity Mission, Sentinel-1) will reduce the uncertainty.

Table 8 summarizes the deviation of all kinds of ground measurement under different landscapes. It gives intuitive information about uncertainty among different *in situ* measurements. The best performance is obtained at the annual scale with a deviation of 3.8%, showing that annual ET is more reliable than ET at a single day or month. While the agreement at the temporal scale was lower, it is still acceptable under plain and sub-urban landscape, especially at time periods of a half month or month. The high accuracy of ET measurements at the field scale was related to heterogeneity of the land surfaces, thus deviation at the Guantao site (homogeneous crop) was relative low both with EC and LAS. At the Daxing site, where vegetable field is mixed with cropland, a high deviation (−13.72%) occurred at the 30 m pixel resolution with EC and a much lower bias (−2.2%) at the 1 km pixel resolution with LAS.

From Table 8, we note that deviation with EC is larger than with other instruments.

5. Discussion

It is widely accepted in the international literature that the measurements of the individual fluxes by an Eddy Covariance system (EC) are not closing. Because the closing errors can be attributed to any flux term of the energy balance (Eq. (1)), the source of the problem is unresolved. A closing error of 15–20% is often accepted as normal (Norman et al., 1995a,b; Wilson et al., 2002). The errors in the measurements are usually ascribed to sampling errors, different footprints for individual energy fluxes, advection, calibration of sensors, loss between low frequency and high frequency measurements, heat storage in the topsoil, and more. The ET flux measured by an eddy covariance system over an irrigated mango orchard in Brazil was likely to have an uncertainty of 18% (Teixeira de Castro and Bastiaanssen, 2012). Sensible, latent, and soil heat flux all need a correction term to obtain a consistent and reliable surface energy balance. This level of accuracy needs to be considered when validating the performance of ETWatch.

A remotely sensed ET image described the ET value of discrete geo-referenced areas. The pixel value represented the average ET value for a 30 m × 30 m area (in case of Landsat) or a 1 km × 1 km area (in case of MODIS). Field measurements of turbulent fluxes

represent a different area, which does not match with areas covered by the pixels. This issue of mismatching scales affected by turbulent procedure holds true for heterogeneous areas and to a lesser extent to areas with homogeneous land use and hydrological conditions.

The goal of ETWatch is to integrate practical models into an operational monitoring system, focusing on several bottlenecks including model applicability in mountainous and urban areas, temporal scaling approach of instantaneous fluxes and disaggregation of ET in semi-humid regional for higher spatial resolution. These features were driven by multi-platform data and can provide better estimation.

For mountainous and urban areas, aerodynamic parameters are quite sensitive to obstacle height and density for different types of land surfaces, due to the variable geometric characteristics, the error can reach several orders of magnitude (Zhang, 2009). The simplified relationship between roughness and vegetation height and empirical value based on a land-use map is limited (Allen et al., 2007). In ETWatch, three factors were taken into account to obtain regional roughness length for momentum transfer z_0 m, including vegetation, topography, and non-vegetation obstacles, to express the region's comprehensive and effective roughness (Wu et al., 2008; Xiong et al., 2010a,b).

In mountainous areas, the temperature lapse rate is another key variable which controls the sensible heat flux simulation of the model. It is fitted from monthly ground data and could be adjusted in a visual interface, according to circumstances. It enables reasonable distribution of sensible heat flux based on water and heat conditions. We fitted the monthly shortwave radiation equations, establishing a lookup spatial map by longitude and latitude based on seven radiation stations located in the Hai Basin. A topographical correction on albedo also contributes to a precise integral estimation of daytime shortwave solar radiation.

Gap-filling and temporal scaling is still the main obstacle in the application and evaluation of ET products. Work is to be done in data-scarcity in order to combine different spatial and temporal scaling methods to develop an effective platform in combination with the ground-flux network and the hydrological modeling approach. The most difficult part in temporal-scaling is the ET estimation during cloudy and rainy weather according to microwave surface temperature and moisture.

A weak element of ETWatch is the used of an inverse distance interpolation procedure in the data processing routine. It is well-known that geostatistical procedures, e.g. kriging, are superior to inverse distance procedures. Their use is necessary however as long as automatic geostatistical procedures are unavailable. We may expect an improved performance of ETWatch if such procedures can be implemented.

Disaggregation of ET value at 1 km resolution for refiner scaling through data fusion is crucial for irrigation management. Although multi-source remote sensing images increase, providing more

information on spatial distribution of ET. This issue is still open: the discrepancy between ET value in different scales requires further investigations. Also computational complexity issues are relevant in application contexts. As a matter of fact, the future improvement of present method is that fusion errors should be analyzed according to ET time series from different time phases.

ETWatch has been developed to integrate the best aspects of the existing algorithms and tune them into an operational monitoring system, focusing on several bottlenecks including model applicability in mountainous and urban areas, temporal scaling approach of instantaneous fluxes and disaggregation of ET in semi-humid regional for higher spatial resolution. A number of modifications have been introduced that were deemed necessary for half-monthly output data with a 1 km grid for the entire basin and a 30 m grid for selected areas of interest. These datasets will be beneficial for the Hai Basin Commission to curtail the declining groundwater tables by means of ET reduction. There were a few parameters calibrated only for Hai Basin, which need to be calibrated again when ETWatch was applied to other regions.

Further study will be carried out to compare simulation results from a distributed hydrological model with remote-sensing estimations at the watershed level. This may help to accelerate the development of application-level data products.

6. Conclusions

The results of ETWatch were validated against soil moisture depletion, lysimeters, eddy covariance and classical water balances. The field scale ET results were obtained from wheat, maize, and cotton fields. The agreement was good for all investigated fields. Seasonal ETWatch values were within 12% of the field measurements (combination of soil moisture and lysimeter measurements). Annual measurements deviated by approximately 6% (combination of lysimeters and eddy covariance). At the village level, deviations reduced to 4%. The soil moisture depletion and lysimeter measurements gave consistent results. The eddy covariance data correlated well with the ETWatch calculations, but eddy covariance data are probably less reliable than ETWatch calculations. The comparison between eddy covariance flux towers and ETWatch shows that the deviation on individual days can be significant. By comparing the ET for a larger group of satellite overpass days, we could not detect any systematic deviation at the China Flux sites. It was concluded that longer time series of eddy covariance measurements are valuable to demonstrate the performance of ETWatch.

For correlations at the catchment scale, the results were also encouraging. The ET volume estimated by ETWatch for a large area of 70,910 km², containing mountains and forests, was 2.8% higher than ET volumes estimated from rainfall-runoff water balance. At the entire Hai Basin scale the deviation was only 1.8%. Considering that field measurements have various shortcomings related to measurement and data interpretation, and considering the acceptable margin of errors displayed in this validation analysis, it is concluded that ETWatch output is reliable and can confidently be used for operational ET management in the Hai Basin.

Acknowledgements

We acknowledge the support from Global Environment Facility. (No. TF053183) and the 'Knowledge Innovation Program' of Chinese Academy of Sciences (No. KZCX1-YW-08-03). Eddy covariance flux tower sites are part of GEF project and CERN networks for Hai River Basin, and we gratefully acknowledge the efforts of researchers at these sites. Research at the Yucheng site was led by Dr. Z. Ouyang and detailed data were gathered by Y. Yu. Part of net

radiation records of Yucheng site was provided by Ms. Y. Liu. The Luancheng site is supervised by Dr. Y. Shen and detailed data were gathered by Ms. Y. Zhang. Dr. S. Liu is Principal Investigator at the Miyun flux site and well-analyzed data was prepared by Dr. Z. Xu and L. Lu, and their assistance in data post-processing is much appreciated. Research at the Daxing site is led by Dr. Y. Liu and detailed data were gathered by Dr. L. Wang. Mrs. Y. Yang and Dr. J. Qi provided intact daily meteorological data and rainfall gauge measurement in Hai River basin. Landsat TM5 data used in the paper were purchased from the ground receive station of remote sensing data.

References

- Allen, R.G., Pereira, L.S., Raes, D., Smith, M., 1998. Crop evapotranspiration, Food and Agriculture Organization of the United Nations, Rome, Italy, 300pp.
- Allen, R.G., Tasumi, M., Morse, A., Trezza, R., 2005. A landsat-based energy balance and evapotranspiration model in Western US water rights regulation and planning. *Irrigation and Drainage Systems* 19 (3–4), 251–268.
- Allen, R.G., Tasumi, M., Trezza, R., 2007. Satellite-based energy balance for mapping evapotranspiration with internalized calibration (METRIC) – Model. *ASCE J. Irrig. Drain. Eng.* 133 (4), 380–394.
- Allen, R.G., Hendriks, J.N.M., Bastiaanssen, W.G.M., Kjaersgaard, J., Irmak, A., 2010. Status and continuing challenges in operational remote sensing of ET, American Society of Agricultural and Biological Engineers (ASABE). In: Proceedings of 5th National Decennial Irrigation Conference, Phoenix, December 5–8, 2010.
- Anderson, M.C., Norman, J.M., Diak, G.R., Kustas, W.P., Mecikalski, J.R., 1997. A two-source time-integrated model for estimating surface fluxes using thermal infrared remote sensing. *Remote Sens. Environ.* 60, 195–216.
- Bastiaanssen, W.G.M., Menenti, M., Feddes, R.A., Holtslag, A.A.M., 1998. The Surface Energy Balance Algorithm for Land (SEBAL): Part 1 formulation. *J. Hydrol.* 212–213, 198–212.
- Bastiaanssen, W.G.M., Noordman, E.J.M., Pelgrum, H., Davids, G., Allen, R.G., 2005. SEBAL for spatially distributed ET under actual management and growing conditions. *ASCE J. Irrig. Drain. Eng.* 131 (1), 85–93.
- Bastiaanssen, W.G.M., Wu, B., Olson, D.C., Liping, J., 2008. Water saving strategies on the northwest China plain. *Stockholm Water Front* 1, 12–13.
- Brutsaert, W., 1999. Aspects of bulk atmospheric boundary layer similarity under free-convective conditions. *Rev. Geophys.* 37, 439–451.
- Castellví, F., Snyder, R.L., 2010. A new procedure based on surface renewal analysis to estimate sensible heat flux: a case study over grapevines. *J. Hydrometeorol.* 11, 496–508.
- Chamberlain, A.C., 1966. Transport of gases to and from grass and grass-like surfaces. *Proc. Roy. Soc. A* 290, 236–265.
- Chen, F., Mitchell, K., Schaake, J., Xue, Y.K., Pan, H.L., Koren, V., Duan, Q.Y., Ek, M., Betts, A., 1996. Modeling of land surface evaporation by four schemes and comparison with FIFE observations. *J. Geophys. Res.* 101 (D3), 148–227.
- Chen, J., Jonsson, P., Masayuki, T., 2004. A simple method for reconstructing a high-quality NDVI time series dataset based on the Savitzky–Golay filter. *Remote Sens. Environ.* 91, 332–344.
- Cleugh, H.A., Leuning, R., Mu, Q.Z., Running, S.W., 2007. Regional evaporation estimates from flux tower and MODIS satellite data. *Remote Sens. Environ.* 106, 285–304.
- Courault, D., Seguin, B., Olioso, A., 2005. Review on estimation of evapotranspiration from remote sensing data: from empirical to numerical modeling approaches. *Irrig. Drain. Syst.* 19, 223–249.
- Crago, R., Brutsaert, W., 1996. Daytime evaporation and the self-preservation of the evaporative fraction and the Bowen ratio. *J. Hydrol.* 178, 241–255.
- David, J.M., Gary, D.C., Richard, K.T., Richard, L.R., Chavez, J.P.S., 2004. Comparison of aerodynamically and model-derived roughness lengths(z₀) over diverse surfaces. *Geinirögikigt* 63, 103–113.
- Dugas, W.A., Fritschen, L.J., Gay, L.W., Held, A.A., Matthias, A.D., Reicosky, C., Steduto, P., Steiner, J.L., 1991. Bowen ratio, eddy correlation and portable chamber measurements of sensible and latent heat flux overirrigated spring wheat. *Agric. Forest Meteorol.* 56, 1–20.
- Farah, H.O., 2001. Estimation of regional evaporation under different weather conditions from satellite and meteorological data, a case study in the Naivasha Basin. Ph.D. Thesis, Wageningen University, Wageningen, The Netherlands, 170pp.
- Farahani, H., Howell, T., Shuttleworth, W., Bausch, W.C., 2007. Evapotranspiration: progress in measurement and modeling in agriculture. *Trans. Am. Soc. Agric. Engr.* 50 (5), 1627–1638.
- Foster, S., Garduno, H., Evans, R., Olson, D., Tian, Y., Zhang, W., Han, Z., 2004. Quarterly aquifer of the North China plain – assessing and achieving groundwater resource sustainability. *Hydrogeol. J.* 12, 81–93.
- Gao, F., Masek, J., Schwaller, M., Hall, F., et al., 2006. On the blending of the Landsat and MODIS surface reflectance: predicting daily Landsat surface reflectance. *IEEE Trans. Geosci. Remot. Sen.* 44, 2207–2218.
- Glenn, E.P., Huette, A.R., Nagler, P.L., Hirschboeck, K.K., Brown, P., 2007. Integrating remote sensing and ground methods to estimate evapotranspiration. *Crit. Rev. Plant Sci.* 26, 139–168.

- Gockede, M., Markkanen, T., Mauder, M., et al., 2005. Validation of footprint models using natural tracer measurements from a field experiment. *Agric. Forest Meteorol.* 135, 314–325.
- Gruhler, C.P., Rosnay, D.P., Kerr, Y., Mougou, E., Ceschia, E., Calvet, J.C., et al., 2008. Evaluation of AMSR-E soil moisture product based on measurements over temperate and semi-arid regions. *Geophys. Res. Lett.* 35, L10405.
- Jia, L., Wang, J., 1999. Estimation of area roughness length for momentum using remote sensing data and measurements in field. *Chin. J. Atmos. Sci.* 23 (5), 61–69.
- Kalma, J.D., McVicar, T.R., McCabe, M.F., 2008. Estimating land surface evaporation: a review of methods using remotely sensed surface temperature data. *Surv. Geophys.* 29, 421–469.
- Khan, S.I., Hong, Y., Vieux, B., Liu, W., 2010. Development and evaluation of an actual evapotranspiration estimation algorithm using satellite remote sensing and meteorological observational network in Oklahoma. *J. Remote Sens.* 31 (14), 3799–3819.
- Kite, G.W., Droogers, P., 1999. Comparing evapotranspiration estimates from satellites, hydrological models and field data. *J. Hydrol.* 229, 2–18.
- Kormann, R., Meixner, F.X., 2001. An analytic footprint model for neutral stratification. *Bound.-lay. Meteorol.* 99, 207–224.
- Kustas, W.P., Anderson, M.C., French, A.N., Vickers, D., 2006. Using a remote sensing field experiment to investigate flux footprint relations and flux sampling distributions for tower and aircraft-based observations. *Adv. Water Res.* 29, 355–368.
- Li, Z.Q., Yu, G.R., Wen, X.F., 2005. Energy balance closure at China FLUX sites. *Sci China. Ser. D.* 48 (Suppl.1), 51–62.
- Liu, S.M., 2010. Independent Ground Validation Report of Remote Sensing Evapotranspiration (ET) in Hai River Basin. Beijing Normal University, School of Geography.
- Liu, C., Yu, J., Kendy, E., 2001. Groundwater exploitation and its impacts on the environment in the North China. *Water Int.* 26, 265–272.
- Liu, S.F., Xiong, J., Wu, B.F., 2011a. ETWatch: a method of multi-resolution ET Data fusion. *J. Remote Sens.* 15 (2), 55–69.
- Liu, S.M., Xu, Z.W., Wang, W.Z., Jia, Z.Z., Zhu, M.J., Bai, J., Wang, J.M., et al., 2011b. A comparison of eddy-covariance and large aperture scintillometer measurements with respect to the energy balance closure problem. *Hydrol. Earth Syst. Sci.* 15, 1291–1306.
- Mao, K., Qin, Z., Shi, J., Gong, P., 2005. A practical split-window algorithm for retrieving land-surface temperature from MODIS data. *Int. J. Remote Sens.* 26 (15), 3181–3204.
- Marquardt, D.W., 1963. An algorithm for least-squares estimation of nonlinear parameters. *J. Soc. Ind. Appl. Math.* 11 (2), 431–441.
- Marx, A., Kunstmann, H., Schuttemeyer, D., 2008. Uncertainty analysis for satellite derived sensible heat fluxes and scintillometer measurements over Savannah environment and comparison to mesoscale meteorological simulation results. *Agric. Forest Meteorol.* 148 (4), 656–667.
- McAneney, K.J., Green, A.E., Astill, M.S., 1995. Large aperture scintillometry: the homogeneous case. *Agric. Forest Meteorol.* 76, 149–162.
- Meijninger, W.M.L., de Bruin, H.A.R., 2000. The sensible heat fluxes over irrigated areas in Western Turkey determined with a large aperture scintillometer. *J. Hydrol.* 229, 42–49.
- Meijninger, W.M.L., Hartogensis, O.K., Kohsiek, W., Hoedjes, J.C.B., Zuurbier, R.M., Bruin De, H.A.R., 2002. Determination of area-averaged sensible heat fluxes with a large aperture scintillometer over a heterogeneous surface – flevoland field experiment. *Bound. Lay. Meteorol.* 105 (1), 37–62.
- Monteith, J.L., 1965. Evaporation and the environment, in: the state and movement of water in living organisms. In: XIXth symposium Soc for xp, Swansea Cambridge University Press, pp. 205–234.
- Mu, Q.Z., Heinsch, F.A., Zhao, M.S., Running, S.W., et al., 2007. Development of a global evapotranspiration algorithm based on MODIS and global meteorology data. *Remote Sens. Environ.* 111, 519–536.
- Norman, J.M., Kustas, W.P., Humes, K.S., 1995a. A two-source approach for estimating soil and vegetation energy fluxes from observations of directional radiometric surface temperature. *Agric. Forest Meteorol.* 77, 163–293.
- Norman, J.M., Kustas, W.P., Humes, K.S., 1995b. Source approach for estimating soil and vegetation energy fluxes in observations of directional radiometric surface temperature. *Agric. Forest Meteorol.* 77, 263–293.
- Qian, Q.J., Wu, B.F., Xiong, J., 2005. Interpolation System for Generating Meteorological Surfaces Using to Compute Evapotranspiration in Haihe River Basin. (IGARSS). IEEE International Geoscience & Remote Sensing, Symposium.
- Schmid, H.P., 1994. Source areas for scalars and scalar fluxes. *Bound. Layer Meteorol.* 67, 293–318.
- Schmid, H.P., 2002. Footprint modeling for vegetation atmosphere exchange studies: a review and perspective. *Agric. Forest Meteorol.* 113, 159–183.
- Shen, Y., Yang, Y., 1998. The effect of agricultural water saving on hydrological cycle: a case study in Luancheng, China. In: Proceedings of International Workshop on Methods of Field Investigation of Water Cycle and China-Japan NCP Project. Shijiazhuang, China, June 1998, pp. 99–105.
- Shen, Y., Zhang, Y., Kondoh, A., Tang, C., Chen, J., Xiao, J., Sakura, Y., Liu, C., Sun, H., 2004. Seasonal variation of energy partitioning in irrigated lands. *Hydrol. Process.* 18, 2223–2234.
- Shuttleworth, W.J., Gurney, R.J., Hsu, A.Y., Ormsby, J.P., 1989. FIFE: the variation in energy partitioning at surface flux sites, remote sensing and large scale global processes. In: Proceedings of Baltimore Symp., IAHS publ. 186. IAHS Press, Oxfordshire, UK, pp. 67–74.
- Soppe, R.W.O., Bastiaanssen, W.G.M., Droogers, P., Immerzeel, W., 2004. Water Savings in the Hai Basin. WaterWatch Report.
- Stein, A., Zaadnoordijk, W.J., 1999. Improved parameter estimation for hydrological models using weighted object functions. *Hydrol. Process.* 13, 1315–1328.
- Su, Z., 2002. The Surface Energy Balance System (SEBS) for estimation of turbulent heat fluxes. *Hydrol. Earth Syst. Sci.* 6 (1), 85–99.
- Su, Z., Schmugge, T., Kustas, W.P., Massman, W.J., 2001. An evaluation of two models for estimation of the roughness height for heat transfer between the land surface and the atmosphere. *J. Appl. Meteor.* 40, 1933–1951.
- Teixeira de Castro, A.H., Bastiaanssen, W.G.M., 2012. Five methods to interpret field measurements of energy fluxes over a micro-sprinkler irrigated mango orchard. *Irrig. Sci.* 30, 13–28.
- Thom, A.S., 1972. Momentum, mass and heat exchange of vegetation. *Quart. J. Roy. Meteorol. Soc.* 98, 124–134.
- Vaughan, P.J., Trout, T.J., Ayars, J.E., 2007. A processing method for weighing lysimeter data and comparison to micrometeorological ET predictions. *Agric. Water Manage.* 88 (1–3), 141–146.
- Vermote, E.F., Tanré, Didier, Deuzé, Jean Luc, Herman, Maurice, Morcette, Jean-Jacques, 1997. Second simulation of the satellite signal in the solar spectrum, 6S: an overview. *IEEE Trans. Geosci. Remote Sens.* 35 (3), 675–686.
- Wan, Z.M., Li, Z.L., 1997. A physics-based algorithm for retrieving land-surface emissivity and temperature from EOS/MODIS data. *IEEE Trans. Geosci. Remote Sens.* 35 (4), 980–996.
- Wilson, K., Goldstein, A., Falge, E., Aubinet, M., Baldocchi, D., Bernhofer, C., Ceulemans, R., Dolman, H., Field, C., 2002. Energy balance closure at Fluxnet sites. *Agric. Forest Meteorol.* 113, 223–243.
- Wu, B.F., Xiong, J., Yan, N.N., 2008. ETWatch: An Operational ET Monitoring System with Remote Sensing. ISPRS III Workshop.
- Wu, B.F., Xiong, J., Lu, S.L., 2009. Estimation and calibration of remote sensed evapotranspiration for Hai River basin. In: Hai River Basin Integrated Management of Water Resources and Environment International Symposium, Beijing.
- Wu, B.F., Xiong, J., Yan, N.N., 2010. ETWatch: models and methods. *J. Remote Sens.* 15 (2), 224–230.
- Wu, B., Xiong, J., Lu, S.L., 2010. Discussion on remote sensed ET validation and land-use accuracy assessment. In: Wen Wurui et al. (Eds.), Haihe River Basins Research and Planning Approach, Proceedings of 2009 International Symposium of Haihe Basin Integrated Water and Environment Management, Orient Academic Forum, pp. 336–342.
- Xiong, J., Wu, B.F., Yan, N.N., Hu, M.G., 2007. Algorithm of regional surface evaporation using remote sensing: A case study of Haihe basin, China. MIPPR: Remote Sensing and GIS data Processing and Applications. In: Proceedings of SPIE, vol. 679025.
- Xiong, J., Wu, B., Yan, N., Zeng, Y., Liu, S., 2010a. Estimation and validation of land surface evaporation using remote sensing and meteorological data in North China. *IEEE J. Selected Top. Appl. Earth Obser. Remote Sens.* 3 (3), 337–344.
- Xiong, J., Wu, B., Liu, S., 2010b. Estimation and calibration of remote sensed evapotranspiration for Hai river basin. In: Wen Wurui et al. (Eds.), Haihe River Basins Research and Planning Approach, Proceedings of 2009 International Symposium of Haihe Basin Integrated Water and Environment Management, Orient Academic Forum, pp. 200–214.
- Xiong, J., Wu, B.F., Liu, S.F., Yan, N.N., Wu, F.M., 2011. ETWatch: calibration methods. *J. Remote Sens.* 15 (2), 240–254.
- Yang, Y.H., Tian, F., 2009. Abrupt change of runoff and its major driving factors in Haihe River Catchment, China. *J. Hydrol.* 374, 373–383.
- Yang, K., Wang, J.M., 2008. A temperature prediction-correction method for estimating surface soil heat flux from soil temperature and moisture data. *Sci. China Ser. D – Earth Sci.* 51 (5), 721–729.
- Zhang, R.H., 2009. Quantitative Model of Thermal Infrared Remote Sensing and Ground based Experiments. Science Press, Beijing.
- Zhang, Y., Liu, C., Shen, Y., Kondoh, A., Tang, C., Tanaka, T., Shimada, J., 2002. Measurement of evapotranspiration in a winter wheat field. *Hydrol. Process.* 16, 2805–2817.
- Zhang, Y., Kendy, E., Qiang, Y., Changming, L., Yanjun, S., Hongyong, S., 2004a. Effect of soil water deficit on evapotranspiration, crop yield and water use efficiency in the North China Plain. *Agric. Water Manage.* 64 (2), 107–122.
- Zhang, Y., Liu, C., Yu, Q., Shen, Y., Kendy, E., Kondoh, A., Tang, C., Sun, H., 2004b. Energy fluxes and the Priestly-Taylor parameter over winter wheat and maize in the North China Plain. *Hydrol. Process.* 18, 2235–2246.
- Zhu, C.Y., Zhang, R.H., Wang, J.F., 2002. The retrieval of aerodynamic surface roughness from SAR remote sensing image. In: First International Symposium on Recent Advances in Quantitative Remote Sensing, Beijing, China.
- Zhu, C.Y., Zhang, R.H., Wang, J.F., Sun, X.M., Zhu, Z.L., 2004. The quantitative retrieval of aerodynamic surface roughness from SAR and thermal remote sensing image Science in China. Ser. D Earth Sci. 34 (4), 385–393.